Grazing-incidence metal deposition: Pattern formation and slope selection

Sebastiaan van Dijken, Louis C. Jorritsma,* and Bene Poelsema
Faculty of Applied Physics and MESA+ Research Institute, University of Twente, P.O. Box 217, NL-7500 AE Enschede, The Netherlands
(Received 15 November 1999)

Molecular beam epitaxy of Cu on Cu(001) at grazing angles of incidence has been studied using spot profile analysis low-energy electron diffraction. At angles of incidence larger than 50° the evolving surface morphology no longer shows the fourfold symmetry inherent to Cu(001), leaving only the plane of incidence as a mirror plane. The surface roughness as well as the slope of the grown mound structures increase with increasing deposition angle. These findings are explained by steering, which originates from long-range attractive forces between incident atoms and substrate atoms and leads to preferential arrival of atoms on top of islands. Steering is of general importance and should routinely be considered in growth studies when the angle of incidence of the depositing beam is larger than 50°.

I. INTRODUCTION

Homoepitaxial growth on single crystal surfaces usually proceeds via nucleation, growth, and coalescence of two-dimensional islands. Atoms originating from a particle beam arrive at the surface, get accommodated at the substrate, and begin thermally activated surface diffusion. Since atom diffusion is the dominant dynamic process on the surface, much effort has been made to determine the rates of the different atom diffusion processes. It has been known for a long time that two diffusion processes play a key role in the evolution of the surface morphology during growth. Atom diffusion on a flat terrace determines the intrinsic lateral length scale of a film during the early stages of growth. On the other hand, the growth mode is controlled by the atom diffusion across descending step edges. For layer-by-layer growth efficient interlayer diffusion is a necessary condition. In the ideal case, one layer is almost completely filled before nucleation and growth in the next layer are initiated. If, however, atom diffusion across descending step edges is suppressed by an additional activation barrier [the Ehrlich-Schwoebel (ES) barrier], growth in the next layer starts long before the previous one is filled and mound structures develop (multilayer or three-dimensional growth).

Compared to atom diffusion, the deposition of atoms on the surface has not been studied in detail. Up to now, growth studies have implicitly regarded the flux of impinging atoms as being homogeneously distributed over the surface. This is remarkable since long-range attractive forces between deposited atoms and substrate atoms lead to substantial deflection of grazing-incident atoms.[1] For the flat surface this phenomenon has no consequences: the refraction of the approaching atoms is the same for all atoms and the incident flux remains homogeneously distributed. However, as soon as adatom islands grow, morphology-dependent atom trajectories give rise to a redistribution of the incident atoms, i.e., the incident atom flux depends on the local surface morphology.

In a recent paper[2] we have shown that refraction of atoms results in preferential arrival on protruding terraces such as islands. In fact, approaching atoms are focused onto the regions next to the front edges of adatom islands. We refer to this phenomenon as *steering.* Steering is most pronounced for grazing-incidence deposition and results in a significantly increased roughness of the growing film. In this paper we will discuss in more detail the influence of steering on pattern formation, kinetic roughening, and slope selection.

To illustrate the steering phenomenon, we report a spot profile analysis low-energy electron diffraction study of the homoepitaxial growth of Cu(001). Normal-incidence growth of Cu/Cu(001) is characterized by the growth and coalescence of two-dimensional square islands. The step edges of the adatom islands are oriented along the close-packed $\langle 110 \rangle$ directions. The distance between the islands is controlled by the activation barrier for diffusion of copper atoms on the (001) terraces (0.36–0.40 eV[3–5]), and the substrate temperature. The development of square islands is favored by the fact that the activation barrier for diffusion of atoms along a step edge is much lower than that of isolated adatoms on a flat terrace.[6] Upon further growth, mound structures develop,[7–10] which order in a quite regular checkerboardlike pattern.[9] The slope orientation of the mound sides depends critically on the growth temperature.[7–9] After normal-incidence deposition, {113}, {115}, and {117} facets have been obtained.

In our Cu/Cu(001) growth experiments, we have deposited copper atoms at different grazing angles of incidence, at different substrate temperatures, and along two different high-symmetry azimuthal directions. The experimental results show that the evolution of the surface morphology is drastically influenced by the deposition geometry. In the submonolayer regime distinct differences in the surface morphology that develops during normal- and grazing-incidence deposition are already observed. During grazing-incidence deposition rectangular adatom islands develop instead of square ones. Upon further growth, symmetrical mound structures, asymmetrical mound structures, and well ordered ripple structures can be obtained, depending on the deposition geometry. Furthermore, the slope of the adatom structures becomes steeper with increasing deposition angle.

This paper is organized as follows. In Sec. II the experimental details are described. In Sec. III the experimental data are presented. First normal-incidence growth and growth at a grazing angle of 80° are compared. Thereafter, the steering effect is discussed and illustrated with atom trajectory calcu-

lations. Then the slopes obtained at different deposition angles are presented. Finally, experimental results for different substrate temperatures and azimuthal deposition directions are given. In Sec. IV the results are discussed. Section V summarizes this work.

II. EXPERIMENTAL DETAILS

The experiments have been performed in ultrahigh vacuum (base pressure $<10^{-10}$ mbar) using spot profile analysis low-energy electron diffraction (SPA-LEED). The transfer width of the SPA-LEED instrument amounts to about 1500 Å . The *ex situ* desulfurized copper crystal has been further prepared in UHV by numerous cycles of sputtering with 800 eV Ar^+ ions and prolonged heating at about 800 K. This preparation method allows standard mean terrace widths of 1000 Å . The deposited copper has been sublimated from a copper disk heated from the rear by means of electron bombardment. Copper atoms have been deposited at normal and grazing angles of incidence along either the [110] or the [100] azimuths. The growth experiments have been performed at three different substrate temperatures (200 K, 250 K, 300 K) with a deposition rate of about 0.25 monolayers per minute. Immediately after deposition the temperature of the copper substrate has been quenched rapidly in order to suppress undesired diffusion. The SPA-LEED data have been acquired with the substrate held at 100 K.

III. RESULTS

A. Normal- versus grazing-incidence deposition

Figure 1(a) shows a profile of the specular beam obtained after normal incidence deposition of 40 monolayers of copper on Cu(001) at 250 K. The spot profile shows a well developed fourfold symmetry as expected for the Cu(001) surface. The observed diffraction pattern can be interpreted straightforwardly as resulting from growth-induced mound structures.[7–10] The distance between mounds after normal-incidence deposition varies between about 25 Å and 250 Å , depending on the temperature of the substrate during copper deposition. The slopes of the mounds are not very well defined and it takes several tens of monolayers before slope selection starts. The slope again depends on the temperature: the average slope decreases from corresponding to {113} facets below 180 K to {117} facets between 280 and 320 K.[7–9] The facet peaks visible in Fig. 1(a) correspond to a {115} slope orientation. Side faces formed by {111} facets have not been detected at all after normal-incidence molecular beam epitaxy (MBE) growth of Cu/Cu(001). The mounds are situated in a quite regular checkerboard pattern with the smallest distance oriented along $\langle 100 \rangle$.[9] The basis for this pattern is already laid during growth of the very first monolayer, just after the onset of coalescence. It has been shown to be a natural consequence of the homogeneous adatom diffusion on Cu(001) combined with the growth of equilibrium shaped (thus, square) islands (see below).

Figure 1(b) shows a SPA-LEED peak profile of the specular beam obtained after growth of 0.5 monolayers of copper at normal incidence. The observed ring around the central (00) beam results from a quite narrow adatom island separation distribution. The homogeneous ring intensity reflects an isotropic radial distribution of adatom islands, caused by the homogeneous adatom diffusion on Cu(001). The fourfold pattern at larger wave vector $k_{//}$ in Fig. 1(b) indicates the square shape of adatom islands which are oriented with their edges along the close-packed $\langle 110 \rangle$ directions. The fourfold pattern is comparable with the optical equivalent of Fraunhofer diffraction from randomly distributed square apertures. The development of square islands is favored by the fact that the mobility of ledge atoms is much higher than that of isolated adatoms on the (001) terraces.[6]

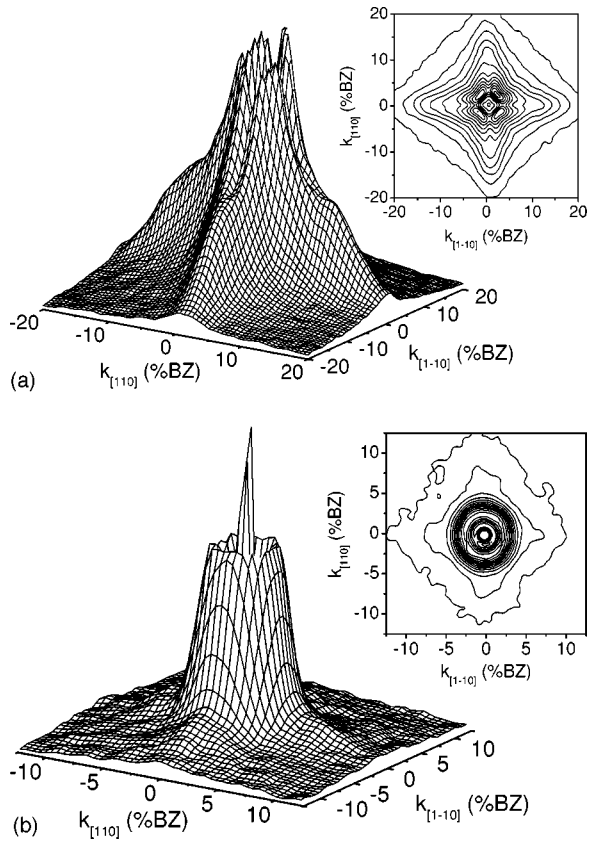

FIG. 1. (a) SPA-LEED peak profile and contour plot of the specular beam acquired after normal-incidence deposition of 40 monolayers copper on Cu(001) at 250 K. The spot profile was obtained at $E=120$ eV (perpendicular scattering phase in units of 2π, $S_z=3.22$). (b) The same for normal-incidence deposition of 0.5 monolayers copper at 250 K: $E=133$ eV ($S_z=3.40$).

In contrast to normal deposition, MBE at grazing incidence destroys the fourfold symmetry of the film morphology. Instead, a twofold symmetric peak profile emerges with the plane of incidence acting as a mirror plane. Figure 2(a) shows a profile of the specular beam obtained after deposition of 40 monolayers of copper on Cu(001) at a grazing angle of 80° with respect to the surface normal. The copper has been deposited along the [110]-azimuth with the substrate at 250 K. The peak profile shows two well developed facet peaks in the plane of incidence of the copper atom beam. Perpendicular to this plane of incidence no distinct diffraction features are measured. The resulting profile is almost one dimensional. The observed asymmetric diffraction pattern is interpreted straightforwardly as resulting from growth-induced parallel ripples at the Cu(001) surface. The orientation of these ripples is perpendicular to the plane of

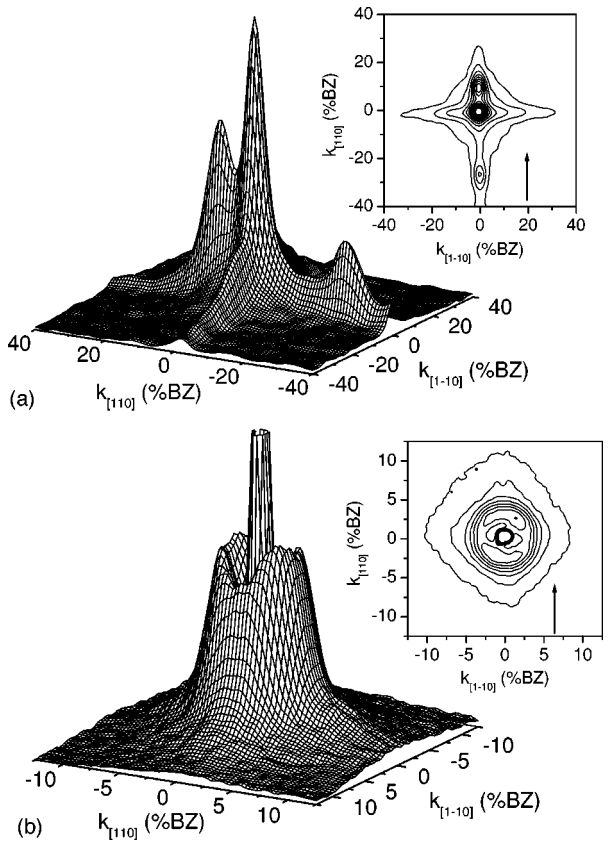

FIG. 2. (a) SPA-LEED peak profile and contour plot of the specular beam acquired after deposition of 40 monolayers copper at an angle of 80° from the surface normal with the Cu(001) substrate at 250 K. The spot profile was obtained at $E=176$ eV ($S_z=3.91$). (b) The same after deposition of 0.5 monolayers copper under identical conditions: $E=133$ eV ($S_z=3.40$). The arrow in the contour plots indicates the deposition direction.

incidence of the copper beam. The ripples are well defined and have an average length of about 500 Å , which can be concluded from the absence of out-of-plane diffraction features and the small out-of-plane width of the facet peaks. The slopes of the ripples on the illuminated and shadow sides have a $(\overline{1}11)$ and (113) orientation, respectively. Compared to normal-incidence deposition, the slopes are much better defined and also substantially steeper. This clearly evidences a substantially enhanced surface roughness after grazing-incidence deposition, compared to the situation after normal-incidence deposition.

The base for the morphology found after growth of 40 monolayers is again already laid during the growth of the first monolayer. Figure 2 (b) shows a SPA-LEED peak profile of the specular beam obtained after growth of 0.5 monolayers of copper at a grazing angle of 80°. The observed ring around the central (00) beam is not rotationally symmetric but exhibits a clearly developed twofold symmetry. This remarkable beam profile with maxima in the deposition plane reflects an isotropic distribution of *rectangular* adatom islands in contrast to *square* adatom islands developing at normal incidence. The rectangular islands are distributed with their long sides perpendicular to the plane of incidence of the copper beam and with their edges oriented along the close-packed ⟨110⟩ directions.

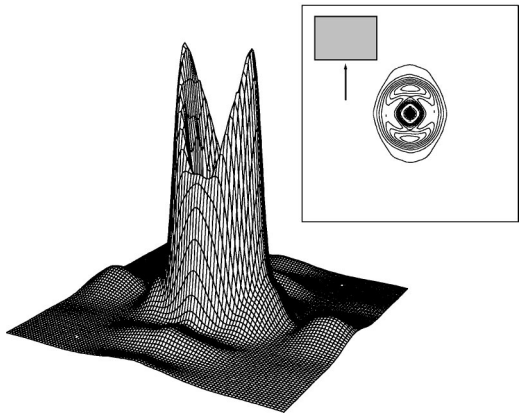

FIG. 3. Calculated quasidiffuse peak profile of a surface with an isotropic island separation distribution of rectangular islands. The aspect ratio of the islands was 3/2 and the island separation was twice the size of the longest side of the islands. The inset shows the orientation of the rectangular islands.

To illustrate that an isotropic distribution of rectangular islands causes a twofold symmetry in the quasidiffuse scattering ring, we have calculated the quasidiffuse peak profile of such an island distribution. The result is shown in Fig. 3. In this two-dimensional calculation the isotropically distributed rectangular islands all have equal sizes and an aspect ratio of 3/2. The longest side of the rectangle is about half the separation between the islands. Just as in the case of square islands, the Fourier transform of the autocorrelation function is a two-dimensional sinc function, but now the widths of the sinc function in the two high-symmetry directions differ from each other. The intensity of the quasidiffuse scattering ring is therefore reduced in the direction where the sinc function has the smallest width, i.e., the direction along which the adatom islands have their longest side. A comparison with the measurement in Fig. 2(b) reveals that the rectangular adatom islands have their long sides oriented perpendicular to the plane of incidence of the copper atom beam. Further calculations indicate that the rectangular islands found after growth at a grazing angle of 80° have an aspect ratio of about 1.05. This ratio is consistent with global estimates on the basis of the observed island distributions.

From Figs. 1 and 2 we can conclude that, compared to normal incidence, grazing-incidence deposition results in the development of rectangular adatom islands instead of square ones in the first monolayer, enhanced surface roughness upon further growth, and the emergence of a ripple structure instead of mounds. Furthermore, the slopes are substantially steeper after grazing-incidence deposition than those obtained after normal-incidence deposition at the same temperature. Another remarkable difference between normal- and grazing-incidence deposition is the degree of order of the distances between the adatom structures. Figure 4 shows a cross section of a specular beam profile along the [110] azimuth, i.e., in the plane of incidence of the copper beam. It was acquired after grazing-incidence deposition of nine monolayers of copper. Next to the narrow central feature, which represents the (00) beam intensity, the profile shows a lot of structure. First it becomes clear that the onset of asymmetry, which at prolonged deposition results in well developed $(\overline{1}11)$ and (113) facets on the illuminated and shadow

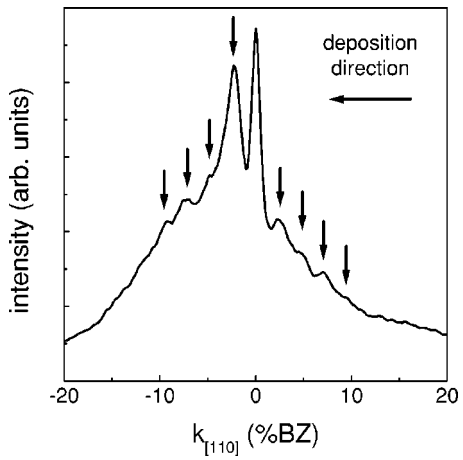

FIG. 4. SPA-LEED specular peak profile in the plane of incidence acquired after deposition of 9 monolayers copper at 80° with the Cu(001) substrate at 250 K. The profile was obtained at $E=116$ eV ($S_z=3.18$). The arrows indicate the first- and higher-order diffraction peaks of the Fourier transform of the island separation function.

sides of the ripples, is already present. The additional peaks reflect the average distance between the adatom islands. Up to fourth-order diffraction features can be distinguished, which is by far more than ever seen at normal-incidence deposition: after normal-incidence deposition only first-order peaks can be detected. This observation reveals that the surface ordering in the plane of incidence of the copper atom beam is highly improved with respect to that obtained after normal-incidence deposition.

The enhanced lateral order at grazing-incidence deposition can be rationalized as follows. For layer-by-layer growth, which initially occurs, the nucleation phase will lead to a rather narrow separation distribution of the adatom islands. As growth at normal incidence proceeds, the separation distribution function related to the centers of gravity of the islands will even narrow quite considerably. This is due to the fact that islands grow fast in the directions in which they are surrounded by extended capture zones, i.e., the directions in which they do not have other islands in their vicinity. On the other hand, island growth in the directions in which islands have other islands in their vicinity is slow. This difference in growth rate causes the centers of gravity of the islands to move in such a way that the average island separation distribution narrows until coalescence sets in. Shortly before coalescence the distribution will be its narrowest. During grazing-incidence growth the azimuthal asymmetry in island growth rate will narrow the island separation distribution as well. An important difference from normal-incidence deposition is the reduced impingement rate in the shadow zones behind the islands. This reduction hampers the coalescence of islands in the plane of incidence: the advance rate of an illuminated step edge is reduced strongly when it enters the shadow zone of a neighboring upstream adatom island. Because of the hampered island coalescence in the plane of incidence, narrowing of the island separation distribution will proceed longer in this direction if the diffusion rate around corners is low. The further developing three-dimensional structures will therefore evolve on a base with a narrower separation distribution in the plane of incidence. Following this scenario the basis for the improved order is again believed to be laid already in the first monolayer. At more advanced stages of growth the situation becomes more complicated, since the lateral variation in the amount of incident copper atoms becomes strongly dependent on the local morphology (see next subsection). Still a quite well defined effective shadow length will be active, which tends to favor enhanced lateral ordering in the plane of the copper atom beam.

B. Steering

The differences in morphology after normal-incidence and grazing-incidence deposition are explained by a phenomenon we introduced recently:[2] *steering-enhanced roughening*. Steering is the focusing of incident atom flux on protruding terraces. It is induced by long-range attractive forces between the substrate and approaching atoms. Thermal energy metal atoms, approaching the surface at typical energies of 0.1 to 0.3 eV, experience long-range attractive forces before they come to rest in a several-eV-deep well. This gives rise to substantial acceleration and in the case of grazing-incidence deposition substantial deflection toward the surface.[1] For a flat substrate this phenomenon has initially no consequences: the incident flux remains homogeneously distributed. The atoms only arrive at an effectively smaller polar angle of incidence, which is determined by the energy of the deposited atoms and the depth of the attractive well in front of the substrate. As soon as aggregates start to build up, however, the redistribution of incident flux becomes progressively more important. Surface roughness causes a distortion in the attractive potential, and therefore atom trajectories are influenced by the local surface morphology. The result is a redistribution of incident atom flux in such away that atoms arrive preferentially on protruding terraces.

To substantiate the phenomenon of steering for different surface morphologies we have performed atom trajectory calculations. In this calculations we have adopted a Lennard-Jones (12,6) pairwise potential, which is given by

$$V(R)=D\left(\frac{\sigma}{R}\right)^6\left[\left(\frac{\sigma}{R}\right)^6-2\right].$$

In this function, σ is the lattice constant (2.55 Å for Cu) and D is a pairwise energy which has been fitted to the cohesive energy ($D=0.4093$ eV for Cu). Normally such a pairwise additive Lennard-Jones potential is inadequate to describe the attractive potential of metals in detail.[11] Sanders and DePristo[12] found, however, that atom trajectory calculations with such a Lennard-Jones potential are satisfactorily close to calculations with their most accurate many-body density-functional-based potential energy surface. We therefore used this potential to calculate the effect of steering semiquantitatively.

Figure 5 shows a cross-sectional view through the Cu(001) substrate along the [110] azimuth. On this substrate we have constructed a one-monolayer-high adatom island. The figure exhibits calculated equipotential energy contours (increment -0.1 eV) as well as three calculated atom trajectories for atoms deposited at a grazing angle of 80°. The equipotential energy contours show substantial distortion in

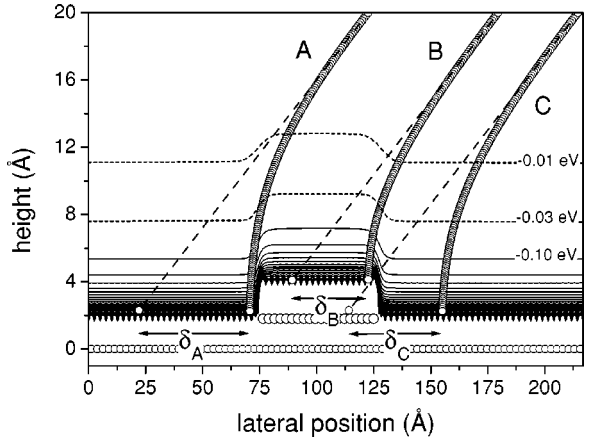

FIG. 5. Calculated equipotential energy contours and three atom trajectories for a surface with a one-monolayer-high island on top of it (note the different length scale on the two axes). The increase in attractive potential is -0.1 eV for the solid contour lines. The trajectory calculations for a deposition angle of 80° start at 20 Å above the surface.

the attractive potential, which is related to the ascending and descending step edges. The lateral length of distortion is about 15 Å for the -0.01 eV contour. Calculations show that 150 meV Cu atoms, deposited with a grazing angle of incidence of 80°, actually hit the surface at an angle of 17°, when the trajectory passes through an undistorted attractive potential (trajectory *C* in Fig. 5). When atoms pass through a distorted attractive potential, however, the trajectories may deviate substantially (trajectory *A* and *B* in Fig. 5). The result of surface-roughness-induced variation in atom trajectories is illustrated most clearly when we consider the distance between the position at which the atoms actually hit the surface and their target point (δ_A, δ_B, and δ_C in Fig. 5). The target point is the intersection of the asymptotic long-distance part of the trajectory with the surface. Atoms following trajectory *A* in Fig. 5 pass through a distorted attractive potential, which is related to a descending step edge. They therefore suddenly experience the surface at a much larger distance and impact is further away. Consequently, the value of δ_A is enhanced with respect to δ_C. The value of δ_A is further enhanced by strong lateral forces between the descending step edge and the approaching slow atom. These two effects give rise to a local reduction of the incident atom flux just behind the adatom island. Atoms following trajectory *B* in Fig. 5, on the other hand, suddenly experience the surface at a much smaller distance when they pass through the distorted attractive potential, which is now related to an ascending step edge. Therefore the actual position of impact is much closer to the target point and δ_B is reduced with respect to δ_C. In addition, the lateral forces between the ascending step edge and the approaching atom reduce δ_B. The consequence is a local enhancement of the incident atom flux just behind the front edge of the adatom island. In fact, all arriving atoms whose trajectories pass through areas of substantial distortion of the attractive potential related to ascending step edges contribute to enhanced flux. They are focused on top of the adatom island, with the maximum atom flux close to the front edge. We refer to this focusing of atom flux on top of adatom structures as steering.

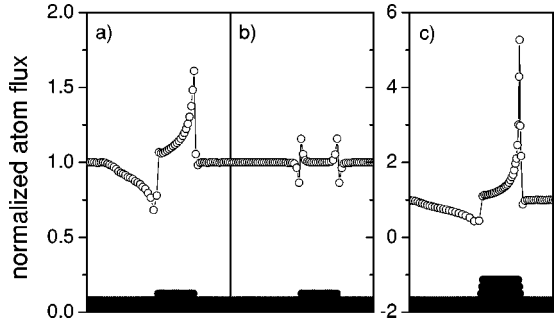

FIG. 6. Calculated atom flux at the surface, normalized to a homogeneous atom flux far above the surface. (a) Surface with a one-monolayer-high island on top of it and a deposition angle of 80°. (b) Surface with a one-monolayer-high island and normal-incidence deposition. (c) Surface with a three-monolayer-high island and a deposition angle of 80°.

We have calculated numerous atom trajectories for different surface morphologies. From these calculations we derived the inhomogeneous atom flux at the surface normalized to the homogeneous flux far above the surface. Three results are shown in Fig. 6. Figure 6(a) shows the calculated normalized atom flux for a surface with a one-monolayer-high adatom island on top of it and deposition at a grazing angle of 80°. The atom flux enhancement factor amounts to about 1.6 at the front of the island and decreases to zero going further downstream on an extended island. Behind the island the flux of the incident atoms is reduced to about 0.7 close to the descending step edge. Note that the atom flux behind the islands never becomes zero and that the range of reduced atom flux ($\approx$60 Å) is much larger compared to classical shadowing without steering (10 Å for deposition at 80°). The reduction of atom flux behind the island compensates the flux enhancement on top of the island, as should be the case for particle conservation reasons.

Figure 6(b) shows the calculated normalized atom flux for the same surface but now for normal-incidence deposition. Obviously, the effect of steering is much smaller for this deposition geometry. Only a small local enhancement of the incident atom flux is observed close to the step edges over a range of just one atom position. The inequality in atom flux redistribution between normal deposition and deposition with a grazing angle of 80° is caused by the substantial difference in atom velocity parallel to the surface. The actual position of impact is very sensitive to small distortions in the attractive potential, when atoms have a relatively large velocity component parallel to the surface. The result is a substantial redistribution of the incident atoms due to morphology-dependent trajectories. On the other hand, deviations in the atom trajectory change the position of impact only slightly when atoms have a small velocity component parallel to the surface. The steering effect is therefore much weaker at normal-incidence deposition.

The influence of surface roughness is illustrated in Fig. 6(c). This figure shows the calculated normalized atom flux for a surface with a three-monolayer-high adatom structure on top of it and deposition at a grazing angle of 80°. While the slopes of the adatom structure correspond to steep {111} facets, the calculated atom flux enhancement can be considered as an upper limit for three-monolayer-high structures.

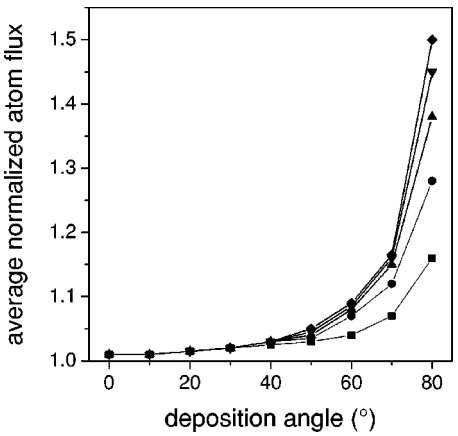

FIG. 7. Average normalized atom flux on top of an adatom structure as a function of the deposition angle. The length of the top layer of the structure is 20 atoms and the structure height is 1 ML, 2 ML, 3 ML, 4 ML, and 5 ML for the square, circle, up triangle, down triangle, and diamond symbols, respectively.

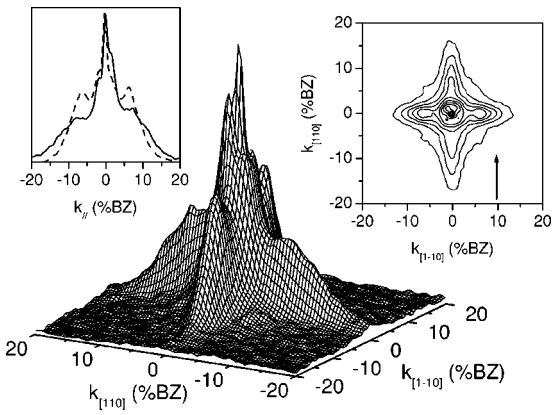

FIG. 8. SPA-LEED peak profile of the specular spot acquired after deposition of 40 monolayers copper at 50° with the Cu(001) substrate at 250 K. The profile was obtained at $E=173$ eV ($S_z=3.87$). The left inset shows line scans through the specular spot in the [110] (solid line) and $[1\bar{1}0]$ (dashed line) directions. The arrow in the right inset indicates the deposition direction.

The atom flux enhancement on top of the adatom structure is obviously much larger compared to that for a one-monolayer-high adatom island. The difference between Fig. 6(a) and Fig. 6(c) is explained by an increased distortion in the attractive potential near the ascending and descending step edges of the three-monolayer-high adatom structure.

The dependence of steering on the deposition angle and adatom structure height is summarized in Fig. 7. This figure shows the *average* normalized atom flux on top of an adatom structure versus deposition angle. The length of the top layer of the adatom structure is 20 atoms. For smaller (larger) adatom structures the average flux enhancement on top will be larger (smaller). Following the calculations, the focusing of atom flux on top of adatom structures is small for deposition angles up to 50°, while steering increases considerably with increasing deposition angle above 50°. The average flux on top of adatom structures also increases rapidly with increasing structure height. The flux enhancement per *additional* monolayer decreases, however. The average atom flux on top of adatom structures saturates for structures about 10 monolayers high.

C. Slope selection

In order to characterize the influence of the deposition angle on the surface morphology we have performed growth experiments at different grazing angles of incidence along the [110] azimuth. In this section we will concentrate on the surface morphology found after deposition of 40 monolayers of Cu on Cu(001) at 250 K. Figure 8 shows a profile of the specular beam obtained after deposition at a grazing angle of 50° with respect to the surface normal. The left inset shows two line scans through this specular beam. The solid line is measured in the [110] direction, i.e., in the plane of incidence of the copper atom beam, while the dashed line is measured perpendicular to this plane of incidence. The two line scans are not identical, as is the case after normal deposition of 40 monolayers of copper. In the plane of incidence of the copper atom beam, the line scan is slightly asymmetric and shows two not very well developed facet peaks. On the other hand, in the perpendicular direction the line scan shows two facet peaks, which are much better developed compared to the facet peaks measured after normal-incidence deposition. The observed diffraction pattern can be interpreted as resulting from growth-induced mound structures. The four sides of the mounds still have a {115} orientation, but now the slopes are better defined in the direction perpendicular to the plane of incidence of the copper atom beam. In the spot profile obtained after growth at an angle of 50° parallel ridges along the ⟨100⟩ directions are not present. These ridges observed after normal-incidence deposition [see Fig. 1(a)] indicate the formation of a checkerboard pattern of mounds.[9] The base for this ordering phenomenon is already laid just after coalescence of the growing adatom islands in the first monolayer. The absence of a checkerboard pattern after growth at 50° therefore suggests that deviations in the surface morphology are already present during the initial stages of growth.

Deposition at an angle between 55° and 70° leads to the formation of asymmetrical mound structures. The sides of the mounds have different slope orientations, which critically depend on the deposition angle. Although not well defined, the average slope at the illuminated side of the mounds increases considerably from 15° [corresponds to a $(\bar{1}\,\bar{1}\,5)$ facet] at a deposition angle of 50° to about 30° at a deposition angle of 65°. Figure 9 shows the position of the facet peaks as a function of the perpendicular scattering phase S_z after growth of 40 monolayers copper at an angle of 70°. Deposition at a grazing angle of 70° results in mounds with an average slope angle of 42° at the illuminated side. After deposition of 40 monolayers copper at an angle between 55° and 70° the shadow sides of the mounds have a well defined slope that is smaller than the slope of the illuminated side. The average slope increases gradually from 15° at a deposition angle of 50° to 23° at a deposition angle of 70°. In contrast to the illuminated and shadow mound sides, the slope increase for the sides perpendicular to the incident copper atom beam is negligible. For deposition angles up to 70° the perpendicular sides have slopes that correspond to {115} facets.

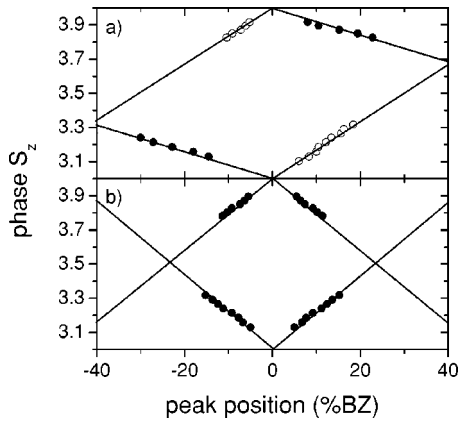

FIG. 9. Position of the facet peaks as a function of the perpendicular scattering phase for the illuminated side [solid circles in (a)], the shadow side [open circles in (a)], and the perpendicular sides [solid circles in (b)] of the mounds measured after deposition of 40 monolayers of copper at 70° with the substrate at 250 K.

As described earlier, deposition at a grazing angle of 80° and 250 K leads to the formation of parallel ripples perpendicular to the incident copper atom beam. The slopes of the ripples on the illuminated and shadow side correspond to $(\overline{1}11)$ and (113) facets, respectively. Perpendicular to the incident copper atom beam, only minor diffraction features are measured. Remarkably, deposition at a grazing angle of 85° again leads to the formation of mound structures. Figure 10 shows a profile of the specular beam obtained after deposition of 40 monolayers copper at 85°. This peak profile shows well developed facet peaks parallel as well as perpendicular to the plane of incidence of the copper atom beam. The four sides of the mounds have a very well defined {111} facet orientation. We note that this slope orientation is never observed after normal-incidence deposition (not even at lower growth temperatures).[7–9] In the spot profile an additional facet peak originating from the shadow side of the mounds is observed. The position of this facet peak follows the rod of the (113) surface in reciprocal space. The shadow side of the mounds therefore consists of (111) and (113) faceted areas.

Figure 11 summarizes the measured slope angles after growth of 40 monolayers copper at 250 K. The error bars in

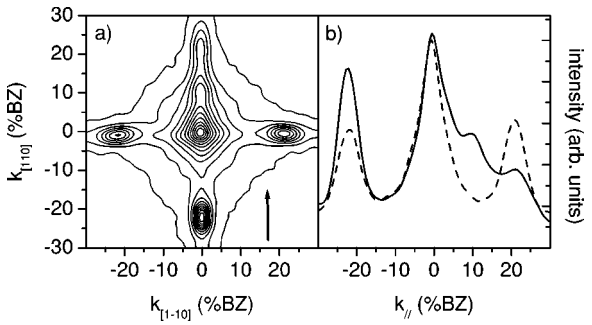

FIG. 10. (a) Contour plot of the SPA-LEED specular beam acquired after deposition of 40 monolayers copper at an angle of 85° from the surface normal with the Cu(001) substrate at 250 K. The profile was obtained at $E=178$ eV ($S_z=3.93$). The arrow indicates the deposition direction. (b) Line scans through the specular spot in the [110] (solid line) and $[1\overline{1}0]$ directions (dashed line).

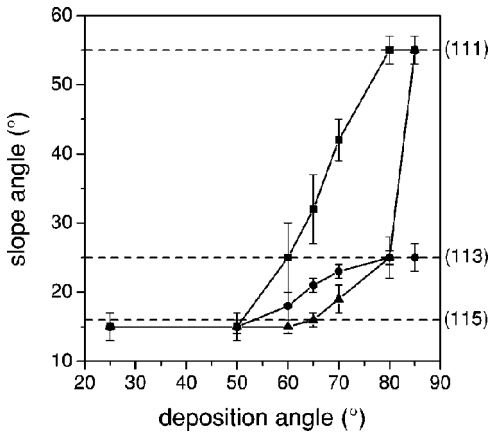

FIG. 11. Measured slope angle after growth of 40 monolayers of copper at 250 K as a function of the deposition angle for the illuminated (squares), shadow (circles), and perpendicular (triangles) sides of the adatom structure.

Fig. 11 are small for well established facets, while somewhat larger error bars result for less well developed facet peaks. In general, the slope angle of all sides of the mound structures increases with increasing deposition angle. At a growth temperature of 250 K slopes corresponding to {115}, {113}, and {111} facets can be obtained.

D. Temperature dependence

Figure 12 shows two SPA-LEED peak profiles of the specular beam obtained after growth of 40 monolayers at a grazing angle of 80° with the substrate at 200 K [(a) and (b)] and 300 K [(c) and (d)], respectively. Both peak profiles show well developed facet peaks in the plane of incidence of the copper atom beam as well as in the perpendicular direction. The observed diffraction pattern is interpreted as result-

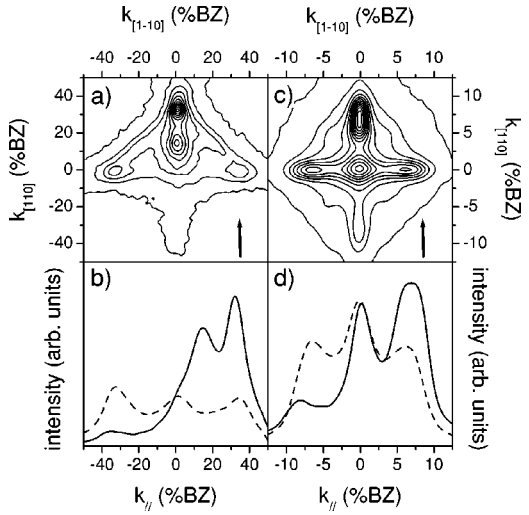

FIG. 12. Contour plots of SPA-LEED peak profiles acquired after deposition of 40 monolayers copper at an angle of 80° from the surface normal with the substrate at 200 K (a) and 300 K (c). The arrows indicate the deposition direction. In (b) and (d) line scans through the specular peak in the [110] (solid lines) and $[1\overline{1}0]$ (dashed lines) directions are shown. The spot profile in (a) and (b) (growth temperature 200 K) was obtained at $E=275$ eV ($S_z=4.88$). The spot profile in (c) and (d) (growth temperature 300 K) was obtained at $E=278$ eV ($S_z=4.91$).

TABLE I. Facet orientation of the sides of the adatom structures measured after normal deposition and deposition at 80° of 40 monolayers copper with the substrate at 200 K, 250 K, and 300 K.

	Normal deposition	Deposition at 80°		
Growth temperature (K)		Illuminated side	Shadow side	Perpendicular sides
200	{113}	$(\overline{1}\,\overline{1}\,1)$	(111) and (113)	{111}
250	{115}	$(\overline{1}\,\overline{1}\,1)$	(113)	{113}
300	{117}	$(\overline{1}\,\overline{1}\,3)$	(113) and (115)	{113}

ing from growth-induced mounds instead of ripples, which are observed after growth at 250 K [see Fig. 2(a)]. The diffraction peak profile obtained after growth at 200 K [Figs. 12(a) and 12(b)] shows two facet peaks originating from the shadow side of the mounds. The positions of these facet peaks follow the rods of the (111) and (113) surfaces in reciprocal space. The average slope of the shadow side is therefore steeper than the slope obtained after normal growth at 200 K or grazing-incidence growth at 80° with the substrate at 250 K [in both cases the slope corresponds to a (113) facet]. The facet peaks in the direction perpendicular to the deposition direction correspond to well established {111} facets. Remarkably, Figs. 12(a) and 12(b) do not show a well defined facet peak originating from the illuminated side of the mounds. In this case, only a faint diffraction feature, which follows the rod of the $(\overline{1}\,\overline{1}\,\overline{1})$ surface in reciprocal space, is visible. The illuminated side of the mounds therefore consists of less well defined (111) facets.

The SPA-LEED diffraction peak profile obtained after growth at 300 K [Figs. 12(c) and 12(d)] shows a well developed facet peak originating from the illuminated side of the mounds. The position of this facet peak follows the rod of the $(\overline{1}\,\overline{1}\,3)$ surface in reciprocal space. The mound slope at the illuminated side is therefore much steeper than the slope obtained after normal growth at 300 K [slope corresponds to a $(\overline{1}\,\overline{1}\,7)$ facet] and less steep than the slope obtained after grazing-incidence growth at 80° with the substrate at 250 K [slope corresponds to a $(\overline{1}\,\overline{1}\,1)$ facet]. One broad facet peak originating from the shadow side of the mounds is measured. Electron-energy-dependent measurements show that the measured broad facet peak actually consists of two separate facet peaks: one originating from (113) faceted areas and the other originating from (115) facets. Therefore, the average mound slope at the shadow side is also less steep than the slope obtained after grazing-incidence growth at 80° with the substrate at 250 K [only a well developed (113) facet peak]. Finally, Figs. 12(c) and 12(d) show clear facet peaks in the direction perpendicular to the plane of incidence of the incident copper atom beam, which correspond to well established {113} facets.

Table I summarizes the mound slopes obtained after deposition of 40 monolayers at 200 K, 250 K, and 300 K. In general, the slope becomes less steep with increasing growth temperature for both normal-incidence deposition and deposition at 80°. Furthermore, the slopes of all facets obtained after grazing-incidence deposition are steeper than those obtained after normal-incidence growth.

E. Azimuthal dependence

In the grazing-incidence growth experiments described so far the deposition was along the [110] azimuth, which is parallel to the direction in which steps of adatom islands are oriented. In order to characterize the influence of the azimuthal deposition direction we have performed grazing-incidence growth experiments along the [100] azimuth. Figure 13 shows a SPA-LEED spot profile of the specular beam obtained after deposition of 40 monolayers of copper on Cu(001) at a grazing angle of 80° with the substrate at 250 K. The observed diffraction pattern is interpreted as resulting from growth-induced mound structures. The facet peaks in the $\langle 110 \rangle$ directions show that the step edges of the adatom structures are still preferentially oriented along the $\langle 110 \rangle$ directions. From this we can conclude that the azimuthal orientation of the mounds does not change with the azimuthal direction of deposition. The facet peaks originating from the shadow sides of the mounds correspond to well established {113} facets. Less well developed {113} facet peaks originating from the two illuminated mound sides are observed as well. The observed average mound slope is again steeper than the slopes obtained after normal growth at 250 K (they correspond to {115} facets). This illustrates that the surface roughness is enhanced after grazing-incidence deposition along the [100] azimuth as well.

IV. DISCUSSION

The evolution of the surface morphology during homoepitaxial growth is governed by two kinetic processes.[13–20] The first process is nucleation during the early stages of monolayer growth. It determines the separation between adatom

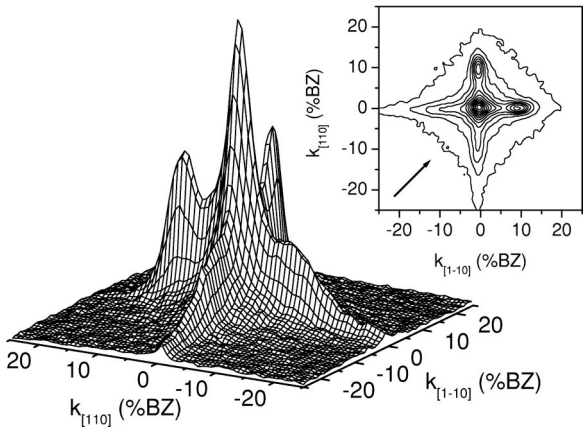

FIG. 13. SPA-LEED peak profile of the specular spot acquired after deposition of 40 monolayers copper at an angle of 80° from the surface normal with the Cu(001) substrate at 250 K. The deposition was along the [100] azimuth, which is indicated by the arrow in the contour plot. The spot profile was obtained at $E=278$ eV ($S_z=4.91$).

islands L, which depends critically on the intralayer diffusion of single adatoms, the deposition rate, and the number of atoms in the smallest stable island.[17,18] Under the usual growth conditions, the density of adatom islands formed during a growth experiment increases with increasing supersaturation, i.e., with decreasing substrate temperature or with increasing deposition rate. The second kinetic process that plays a key role in the evolution of the surface morphology is the interlayer diffusion of adatoms. This process can be quantified by the critical island radius R_c at which nucleation on top of growing islands begins.[16,20] The critical island radius depends on the growth temperature and the height of the activation barrier for downward diffusion at a step edge. The activation barrier for atoms to cross a descending step edge is higher than the activation barrier for diffusion on a flat terrace in most growth systems. The additional barrier E_s, often called the Ehrlich-Schwoebel barrier,[21,22] can therefore be regarded as a reflecting barrier at the step edge. The probability for an adatom to be reflected at a step, following its attempt to descend, increases as $[1-\exp(-E_s/kT)]$. Lowering the growth temperature therefore increases the atom density on top of growing islands. For finite values of E_s this gives rise to enhanced nucleation, i.e., the critical island size R_c at which nucleation on top of islands begins decreases.

When growth proceeds via homogeneous nucleation of adatom islands on flat terraces the growth is characterized by two length scales: the distance between adatom islands L and the critical island radius R_c. No stable nuclei are formed on top of adatom islands before coalescence if R_c is larger than half the separation between adatom islands. In this case the growth mode is called layer by layer and the surface roughness after growth is small. On the other hand, if R_c is smaller than half the separation between adatom islands, nucleation on top of islands occurs before coalescence. Now the growth is three dimensional or multilayer and mound structures are formed.

Homoepitaxial growth will proceed layer by layer in a broad temperature range if there is no step edge barrier. The key point in understanding the growth behavior is that the ability of adatoms to descend from islands is not determined by their ability to reach the island edge. In fact, on the average, every deposited atom on top of an island has sufficient time to reach the island edge before it is captured by other adatoms. This is guaranteed by the length scale (L) set during the nucleation process. Nucleation ceases when an atom deposited between adatom islands has a higher probability to reach the islands than to meet other adatoms to form a new nucleus. An adatom can travel freely at least a distance roughly equal to half the distance between island centers. Since the average island radius before coalescence is always smaller than the average distance between island centers, an adatom on top of an island has the ability to reach the island edge before meeting other atoms deposited on the same island. Therefore, if no significant step edge barrier is present, the adatom density on top of an island will always be less than required for nucleation and no stable nuclei will be formed before coalescence, resulting in layer-by-layer growth.

The presence of a finite step edge barrier leads to multilayer growth. Reflection of adatoms at the island edges results in an enhanced atom density on top of islands and therefore in enhanced nucleation. As a result the critical island radius R_c decreases. While R_c decreases more rapidly than L with decreasing growth temperature[20] a transition from layer-by-layer growth to multilayer growth will occur at a growth temperature at which $R_c \approx 0.5L$. It is thus the step edge barrier that is primarily responsible for deviations from layer-by-layer growth.

The influence of steering on the evolution of the surface morphology can now be discussed. Steering gives rise to a heterogeneity of the incident atom flux, i.e., redistribution of the incident atoms due to their morphology-dependent trajectories. Because of steering, atoms arrive preferentially on protruding terraces. It therefore always enhances the adatom density on top of growing islands. This leads in a very basic way to a decrease of the critical island radius R_c and thus to enhanced roughening of the growing surface, i.e., steering shifts the growth mode from layer-by-layer growth toward multilayer growth. The ultimate consequence of steering is that in principle layer-by-layer growth is never possible. This holds even for a vanishing step edge barrier as some steering effect is always present (even for normal incidence). We explicitly emphasize the point that $R_c < 0.5L$ always, since it is an important and general aspect of this phenomenon in growth. This statement definitely holds in a very basic way, but is on the other hand of rather academic interest: the incident flux enhancement is by definition located near the descending step edges and most of the excess adatom density will disappear easily by interlayer mass transport to the lower terrace.

Interlayer mass transport is less effective in the presence of a step edge barrier. This gives rise to a pronounced enhancement of the adatom density on top of growing islands and therefore to a prominent decrease of the critical island radius R_c.[23] The presence of a finite step edge barrier will thus give rise to multilayer growth even if we disregard steering. The lateral size of the islands in higher levels decreases with increasing altitude. Both effects, i.e., decreasing lateral sizes and increasing height differences, lead to stronger steering-effects. Consequently, steering-induced surface roughening is more effective in the presence of a finite step edge barrier.

The temperature dependence of steering-enhanced roughening is partly controlled by the temperature dependence of interlayer mass transport. For a fixed step edge barrier height, the interlayer mass transport is reduced when the growth temperature is lowered. The influence of steering on surface roughening therefore increases with decreasing growth temperature. As well as this interlayer-diffusion-related temperature effect, there is another temperature effect, which is related to the lateral length scale of the growing film. Intralayer diffusion determines the density of nuclei and thus the separation between adatom islands. This island separation and thus the average island size at a given coverage decrease exponentially with the growth temperature until a temperature is reached at which adatom diffusion is negligible. The relative atom flux enhancement on top of islands is largest for small adatom islands. Steering-enhanced roughening therefore increases strongly with decreasing island size, i.e., with decreasing growth temperature. From this we can conclude that both the step-edge-barrier-related temperature effect and the island-size-related temperature effect re-

sult in an enhanced influence of steering on the surface morphology with decreasing temperature. In addition to the growth temperature, the deposition rate influences steering-enhanced roughening as well. In general, the adatom island density on a surface and thus steering-enhanced roughening increase with increasing deposition rate.

Up to now, growth models have always regarded the flux of impinging atoms as being homogeneously distributed over the surface. The experimental results and the discussion above show that, in addition to intralayer and interlayer diffusion, steering may have an important influence on the morphology of the growing film. Due to steering the incident atom flux is no longer homogeneous. The inhomogeneity in the incident atom flux increases with increasing deposition angle, with increasing surface roughness, and with decreasing growth temperature. In the following we will concentrate on the influence of steering on the selection of the slope angle. Before steering effects are taken into account, slope selection without steering will be discussed.

As outlined above, mounds will be formed during growth in the presence of a finite step edge barrier. These mounds coarsen slowly in time while the sides of the mounds turn into facets. Continuum models[24,25] as well as Monte Carlo simulations[26–29] have been used to describe slope selection. An important parameter in slope selection is a net upward current in the presence of a step edge barrier. The step edge barrier causes preferential incorporation of diffusing adatoms at ascending step edges, defined as a net upward current. Step-adatom attraction found by Wang and Ehrlich[30] may also contribute to a net upward current. The net upward current alone, however, does not lead to slope selection. Slope selection requires a counterbalancing downward current, which results from leakage through the ES barrier or ultimately may be due to downward funneling dynamics.[31,32] Other processes such as transient mobility and knockout events at step edges would have an even greater propensity for smoothening. Molecular dynamics studies, however, suggest that these events are not significant.[12,31] The selected slope is determined by the balance between the upward and downward currents. Larger upward currents, for instance, caused by a significant step edge barrier, lead to steeper slopes.[24–29] On the other hand, a small mound angle will result when the upward current is significantly counteracted by a downward current.

Steering causes a redistribution of the incident atom flux, which depends critically on the local surface morphology. In general, the redistribution of incident flux in favor of protruding terraces will increase during growth (steering increases with increasing roughness or, in other words, roughening is autocatalytic). Due to steering the amount of atoms deposited on the higher terraces is larger than the amount of atoms deposited on the lower terraces. A part of the deposited atoms is incorporated at the ascending step edges. Steering, therefore, drastically enhances the amount of incorporated atoms in the higher layers and thus leads to a larger slope angle. Figure 11 shows that this is indeed the case. The slope angle of the mound/ripple structures increases monotonically with the deposition angle. In other words, the selected slope depends critically on the amount of steering.

Figure 11 shows that different slope orientations can be obtained at one and the same growth temperature. This illustrates that slope selection is not determined by a global thermodynamic equilibrium. Slope selection clearly has a kinetic origin instead. The slope angle is determined by kinetic processes on the surface and the deposition geometry, in which steering plays an important role. The observed temperature dependence of the slope angle for grazing-incidence deposition (see Table I) can be rationalized as follows. The average size of adatom structures on the surface and the interlayer mass transport decrease with decreasing growth temperature. Therefore, the atom flux on top of the adatom structures increases with decreasing growth temperature, which results in steeper facets. The observed temperature dependence of the slope angle for normal incidence deposition (Refs. 7–9 and Table I) may also be explained by steering. Though small, steering still causes a redistribution of atom flux near step edges and thus steeper facets may be obtained at low growth temperatures. The exact influence of steering on the temperature dependence of slope selection is not clear, however, and is probably small under normal-incidence growth conditions. Also, without steering an increase in slope angle with decreasing temperature has to be expected. In the presence of an Ehrlich-Schwoebel barrier, the preferential incorporation of diffusing adatoms at ascending step edges increases with decreasing growth temperature, since the leakage through the barrier is reduced. Therefore, the net upward current is enhanced and steeper slope angles are obtained at lower growth temperatures.

In some growth experiments two facet peaks originating from the shadow side of the mounds are measured. For deposition at 80° two facet peaks are found after growth at 200 K and 300 K, while deposition at 85° results in a shadow side with two slope orientations at 250 K. The formation of two different facets at the shadow side of the mounds may be rationalized as follows. Initially the amount of steering is relatively small. Therefore, the enhancement of incident atom flux on top of islands is sizable only in the regions just behind the front edge. In this situation, the flux enhancement close to the edges on the shadowed sides is negligible. With increasing surface roughness, however, the range of enhanced incident atom flux increases (see Fig. 6) and more atoms will be deposited on the back side of islands as well. This effect is further enhanced because of smaller lateral mound sizes in the higher layers. The additional deposited atoms will be incorporated at step edges in the higher layers, resulting in a larger net upward current. Following this scenario, the facet angle will increase with increasing surface roughness, i.e., increasing amount of deposited atoms. Double-faceted shadow faces may develop, with the high facet being steeper than the facet at the base of the mounds.

As the experimental results show, different surface patterns can be obtained at one and the same growth temperature. Grazing-incidence deposition of Cu/Cu(001) at 250 K leads to the formation of symmetrical mound structures at deposition angles up to 50°, asymmetrical mounds at deposition angles between 50° and 70°, well ordered ripple structures at a deposition angle of 80°, and mounds with very steep faces at a deposition angle of 85°. These remarkable changes from mounds to ripples and back from ripples to mounds can be explained by the existence of two length scales: the separation between adatom structures and the range of reduced incident atom flux behind adatom structures

(shadow length). The separation between adatom structures is determined by the activation barrier for atom diffusion on the (001) terraces and the growth temperature and is by its nature quite well defined. The range of reduced incident atom flux is obviously controlled by the deposition angle and the height of the adatom structures and consequently less well defined. When the range of reduced incident atom flux is smaller than the separation between adatom structures (small deposition angles), mound structures will develop. At larger shadow lengths, however, the coalescence of adatom structures in the deposition direction is suppressed, or better retarded. When the range of reduced incident flux is smaller than the distance between adatom structures, coalescence is still possible in the direction perpendicular to deposition. In this case ripples can develop, which are oriented perpendicular to the plane of incidence of the atom beam. A further increase of the shadow length seems to suppress the coalescence of adatom structures in the direction perpendicular to the deposition direction as well. In this situation, mounds instead of ripples are formed. The speculative scenario for pattern formation during grazing-incidence deposition can be checked by taking a look at the experimental results at different growth temperatures. Deposition at a grazing angle of 80° results in mound structures at 200 K and 300 K, while ripples are obtained at 250 K. Following the scenario outlined above, ripples are expected at a smaller deposition angle when growth proceeds at a lower substrate temperature. At low growth temperatures, the separation between adatom structures is small and a relatively small shadow length, and thus small deposition angle, is enough to suppress coalescence in the deposition direction. For higher growth temperatures this argument leads to an expected ripple structure at a larger deposition angle. Further experiments are underway to check this scenario.

V. CONCLUSIONS

The influence of the deposition geometry on the evolution of the surface morphology during molecular beam epitaxy of Cu/Cu(001) has been studied at substrate temperatures between 200 and 300 K. The growth fronts become progressively rougher upon rotation of the molecular beam from normal to more grazing incidence. The remarkable kinetic roughening observed after growth at grazing incidence can be rationalized in terms of steering. Steering is a direct consequence of long-range attractive forces between the incident atoms and the surface and has so far been overlooked in growth studies. It leads to a redistribution of incident flux: the incident particles are directed preferentially toward protruding terraces, at the cost of flux reduction on lower terraces. In general, steering shifts the growth mode from layer by layer toward three dimensional. Calculations reveal that steering increases with angle of incidence (defined with respect to the normal) and becomes sizable for MBE growth at angles larger than 50°. Steering becomes more important for higher adatom structures, i.e., with proceeding deposition: kinetic roughening is autocatalyzed.

Most of the experiments have been performed with the (MBE) plane of incidence oriented along the [110] azimuth. The deposition of 40 monolayers of Cu leads to different surface morphologies. At normal incidence fourfold symmetric mounds develop, arranged in a checkerboardlike pattern. When the angle of incidence is increased up to about 50° this pattern disappears, leaving symmetric mounds still intact. At more grazing incidence asymmetric mounds evolve, with the exception of a limited angular window in which ripples develop, oriented perpendicular to the molecular beam. The facets of the grown adatom structures are steeper after deposition at more grazing angles of incidence. At 250 K slopes corresponding to {111}, {113}, and {115} facets may be obtained. This fact reflects the kinetic origin of slope selection. The observed facets are steeper for deposition at lower substrate temperatures. The experimental findings, including the temperature dependence, can be explained in a relatively simple picture involving the action of steering combined with two length scales set by nucleation on the flat surface and on top of islands.

Steering-induced kinetic roughening is generic in growth experiments. Its consequences should be anticipated in hetero- as well as in homoepitaxy and are expected to be more important in highly polarizable deposits and substrates. The evolving morphology bears a definite signature of off-normal deposition already at polar angles of incidence of about 50°, a quite normal situation in experimental configurations. This feature should be taken into account whenever comparison between experiments and/or experiment and theory is undertaken.

*Present address: ASML, P.O. Box 324, NL-5500 AH Veldhoven, The Netherlands.

[1] D.E. Sanders, D.M. Halstead, and A.E. DePristo, J. Vac. Sci. Technol. A **10**, 1986 (1992).
[2] S. van Dijken, L.C. Jorritsma, and B. Poelsema, Phys. Rev. Lett. **82**, 4038 (1999).
[3] J.J. de Miguel, A. Sanchez, A. Cebollada, J.M. Gallego, J. Ferrón, and S. Ferrer, Surf. Sci. **189/190**, 1062 (1987).
[4] M. Breeman and D.O. Boerma, Phys. Rev. B **46**, 1703 (1992).
[5] H. Dürr, J.F. Wendelken, and J.-K. Zuo, Surf. Sci. **328**, L527 (1995).
[6] M. Breeman, G.T. Barkema, and D.O. Boerma, Surf. Sci. **303**, 25 (1994).
[7] H.-J. Ernst, F. Fabre, R. Folkerts, and J. Lapujoulade, Phys. Rev. Lett. **72**, 112 (1994).
[8] H.-J. Ernst, F. Fabre, R. Folkerts, and J. Lapujoulade, J. Vac. Sci. Technol. A **12**, 1809 (1994).
[9] L.C. Jorritsma, M. Bijnagte, G. Rosenfeld, and B. Poelsema, Phys. Rev. Lett. **78**, 911 (1997).
[10] J.-K. Zuo and J.F. Wendelken, Phys. Rev. Lett. **78**, 2791 (1997).
[11] D.P. Jackson, in *Interatomic Potentials and Simulations of Lattice Defects*, edited by P. C. Gehlen, J. R. Beeler, Jr., and R. I. Jaffee (Plenum, New York, 1972), and references therein.
[12] D.E. Sanders and A.E. DePristo, Surf. Sci. **254**, 341 (1991).
[13] A.A. Chernov, J. Cryst. Growth **42**, 55 (1977); *Modern Crystallography III* (Springer-Verlag, Berlin, 1984).
[14] B. Lewis and J.C. Anderson, *Nucleation and Growth of Thin Films* (Academic, New York, 1978).
[15] S. Stoyanov and D. Kashchiev, in *Current Topics in Material Science*, edited by E. Kaldis (North-Holland, Amsterdam, 1981), Vol. 7, p. 69.

[16] S. Stoyanov and I. Markov, Surf. Sci. **116**, 313 (1982).
[17] J.A. Venables, Phys. Rev. B **36**, 4153 (1987); Philos. Mag. **27**, 693 (1973).
[18] J.A. Venables, G.D.T. Spiller, and M. Hanbücken, Rep. Prog. Phys. **47**, 399 (1984).
[19] G. Rosenfeld, R. Servaty, C. Teichert, B. Poelsema, and G. Comsa, Phys. Rev. Lett. **71**, 895 (1993).
[20] J. Tersoff, A.W. Denier van der Gon, and R.M. Tromp, Phys. Rev. Lett. **72**, 266 (1994).
[21] G. Ehrlich and F.G. Hudda, J. Chem. Phys. **44**, 1039 (1966).
[22] R.L. Schwoebel and E.J. Shipsey, J. Appl. Phys. **37**, 3682 (1966).
[23] The number of adatoms per surface cell of area a^2 on top of a slow growing island at a distance r from the center is given by $\eta(r)=(F/4D)a^2(R^2+R2a/\alpha-r^2)$, (Ref. 20), where F is the incident atom flux, D is the diffusion constant, R is the island radius, and α varies with temperature as $\exp(-E_s/kT)$. Steering increases the incident atom flux F and thus $\eta(r)$. From the equation it is clear that steering increases the adatom density on top of an island most when E_s/kT is large.
[24] M. Siegert and M. Plischke, Phys. Rev. Lett. **73**, 1517 (1994).
[25] M. Siegert and M. Plischke, Phys. Rev. E **53**, 307 (1996).
[26] J.G. Amar and F. Family, Phys. Rev. Lett. **77**, 4584 (1996).
[27] J.G. Amar and F. Family, Phys. Rev. B **54**, 14 742 (1996).
[28] M.C. Bartelt and J.W. Evans, Phys. Rev. Lett. **75**, 4250 (1995).
[29] M.C. Bartelt and J.W. Evans, in *Evolution of Epitaxial Structure and Morphology*, edited by A. Zangwill, D. Jesson, D. Chambliss, and R. Clarke, MRS Symposia Proceedings No. 399 (Materials Research, Society, Pittsburgh, 1996), p. 89.
[30] S.C. Wang and G. Ehrlich, Phys. Rev. Lett. **70**, 41 (1993).
[31] J.W. Evans, D.E. Sanders, P.A. Thiel, and A.E. DePristo, Phys. Rev. B **41**, 5410 (1990).
[32] Funneling might be regarded effectively as an exception to a homogeneously distributed incident atom flux, since atoms impinging near a descending step come to rest at the lowest level having three, four, or five nearest neighbors below them for fcc (111), (001), and (011), respectively. This obviously leads to a net downward current and thus to smoothing.